Large electronic-density increase on cooling a layered metal: Doped Bi_2Te_3

G. A. Thomas, D. H. Rapkine, R. B. Van Dover, L. F. Mattheiss, W. A. Sunder, L. F. Schneemeyer, and J. V. Waszczak
AT&T Bell Laboratories, Murray Hill, New Jersey 07974
(Received 16 December 1991)

We have carried out optical and transport measurements of the free carriers and optical measurements of states above the semiconducting energy gap in the layered crystal Bi_2Te_3. We find that cooling causes a substantial amount of spectral weight to condense from the above-gap states into the metallic states.

The properties of metallic systems formed by degenerate doping of layered semiconductors[1,2] has proved interesting because such systems can form metals with unusual properties and superconductors with high critical temperatures. One of the simple, fundamental properties of these metals is the spectral weight,[3] which measures the ratio of the carrier density to its mass. In many examples of such materials, this weight is apparently a simple constant,[2–4] as a function of temperature, as expected for most metals. However, in principle, both the electronic density and the effective mass can change. For example, the electronic density can decrease drastically with cooling in the well-known phenomenon of carrier freeze-out lightly doped semiconductors,[5] and it can also decrease when charge-density waves form.[1] In contrast to these constant or decreasing densities, we find an increasing density in the zero-frequency mode. This sort of increase in the density of a metal is rarely seen, but has been observed in the Hall density[6] and to some extent in the optical absorption[7] of degenerately doped semiconductors. We also see a decrease in the spectral weight of states near the energy gap in Bi_2Te_3. We find, therefore, a spectral condensation of nonconducting states into metallic states. During this condensation, the free-carrier density doubles, the predominantly inelastic scattering drops by a factor of 10, and the direct and indirect energy gaps become resolved.

We have produced a metallic band of holes by doping this layered semiconductor[6–13] with excess Bi during the Czochralski growth process.[14] The material crystallizes in a five-layer sandwich structure (Te-Bi-Te-Bi-Te) with rhombohedral symmetry[15] [D^5_{3d} ($R\bar{3}m$) space group], and cleaves easily along the van der Waals bonds between sandwiches to form mirror-quality faces.

The spectral weight in the zero-frequency mode is defined by the square of its plasma frequency. We estimate this frequency directly from minima in our reflectivity spectra shown in Fig. 1(a). The reflectivity R of one of our crystals is plotted over the lower part of the frequency range that we have measured. The R data were obtained by shining light from a Fourier-transform spectrometer onto a large ($\sim 3\times 3$ cm^2) face of the crystal at an angle of incidence near normal (12°). The reflected intensity was compared with that from a Au mirror reference, and the result was corrected for the reflectivity of the gold. These minima in R are classic indications[4] of the screened plasma frequency ω_{Ps} of a degenerate gas of carriers, and the increase of ω_{Ps} as the temperature T decreases can be seen immediately. We have measured two crystals with slightly different doping densities and find the same results.

To fix ω_{Ps} accurately, we fit the region near the minimum in R using[2–4] the Drude form for the complex dielectric function ϵ,

$$\epsilon=\epsilon_H=\omega_{Ps}^2/(E^2+iE/\Gamma) , \quad (1)$$

where ϵ_H is the dielectric constant of the bands at higher energy in the host semiconductor, Γ is the scattering rate, and E is the photon energy. We take Γ as a constant, assuming[3,16] that the predominant inelastic scattering is due to phonon modes which occur[12,13] mainly at E well below ω_{Ps}. These fits are shown in Fig. 1(a) as solid lines, and indicate that, although the constant-Γ approximation is not exact, the fit is adequate for determining ω_{Ps}. As T decreases from 300 to 10 K, fitted values of the spectral weight, ω_{Ps}^2 drop by a factor of 2. We use a constant $\epsilon_H=90$ for the fits.

As the spectral weight in the metal increases, we find that the scattering is predominantly inelastic (there is only a small, constant contribution to Γ as $T\rightarrow 0$)—a surprising result, since we expect[5] strong elastic scattering from the impurity atoms in a doped semiconductor if the dopant atoms are randomly distributed in the lattice. The values of Γ from the fits decrease with decreasing T by a factor ~ 7 (from 22 ± 1 meV at $T=300$ K), and a similar decrease (by ~ 10) is also seen in the dc resistivity ρ, plotted in the inset to Fig. 1(b). We suggest that the elastic-scattering cross section is small because the excess Bi preferentially occupies the central Te(1) sites in the Te(2)-Bi-Te(1)-Bi-Te(2) sandwiches. According to the band-structure results that are presented below, the valence-band states near the Bi_2Te_3 Fermi level have minimal Te(1) character, so that reduced scattering effects can be expected if impurities are substituted at these sites. Furthermore, other elements can be substituted[15] easily at these sites (as in Bi_2Te_2S). If this supposition of doping at the Te(1) site is correct, these materials are natural, modulation-doped heterostructures with doping concentrated in a single layer (δ doped).

We argue that the increase in spectral weight involves a carrier density increase, based on a comparison of the values of ω_{Ps}^2 with our measurements of the Hall density. We obtain the ratio of the metallic density n to the effective mass m spectroscopically from ω_{Ps}^2 using

$$nm_e/m = \omega_{Ps}^2 m_e \epsilon_H / e^2 , \quad (2)$$

where m_e is the free-electron mass and e is its charge. Figure 1(b) shows the ratio nm_e/m as a function of T, where the open circles show the results for the sample shown in Fig. 1(a) and the open squares show the results for a second sample with slightly lower doping density. Both samples show a near doubling of this normalized density. For comparison, we have also measured the Hall density n_{Hall} using conventional dc transport methods.[6–11] The temperature dependence of n_{Hall} is the same as nm_e/m within our experimental uncertainties, but the difference in magnitudes (right and left scales) is about a factor of 10. We conclude from this comparison (and the factor-of-2 correction to n_{Hall} from anisotropy) that the effective-mass ratio[9] m/m_e is 1/5, and that m is roughly T independent. This m/m_e is similar to the value (0.106) determined from the T dependence of the

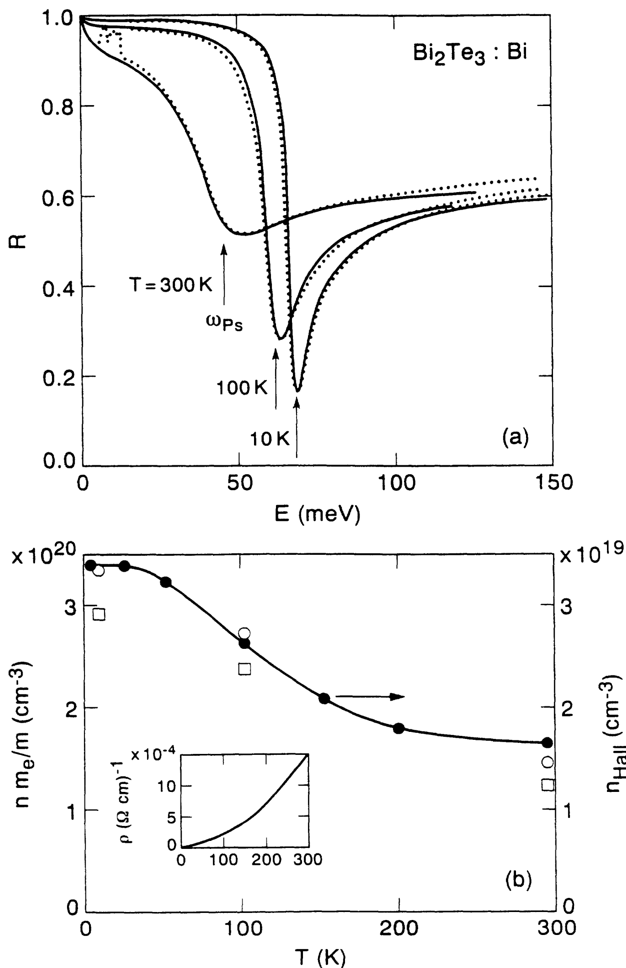

FIG. 1. (a) Reflectivity R for Bi_2Te_3:Bi as a function of photon energy E at three temperatures T. The dots are data and the curves are fits to determine values of the screened plasma frequency ω_{Ps}, which are indicated by arrows. (b) Comparison between (i) the normalized carrier density nm_e/m for two crystals (open circles and squares, left scale) determined from ω_{Ps}, and (ii) values of the Hall density n_{Hall} (closed circles, right scale) as functions of T. The solid curve is a guide to the eye. The inset shows the resistivity, ρ vs T.

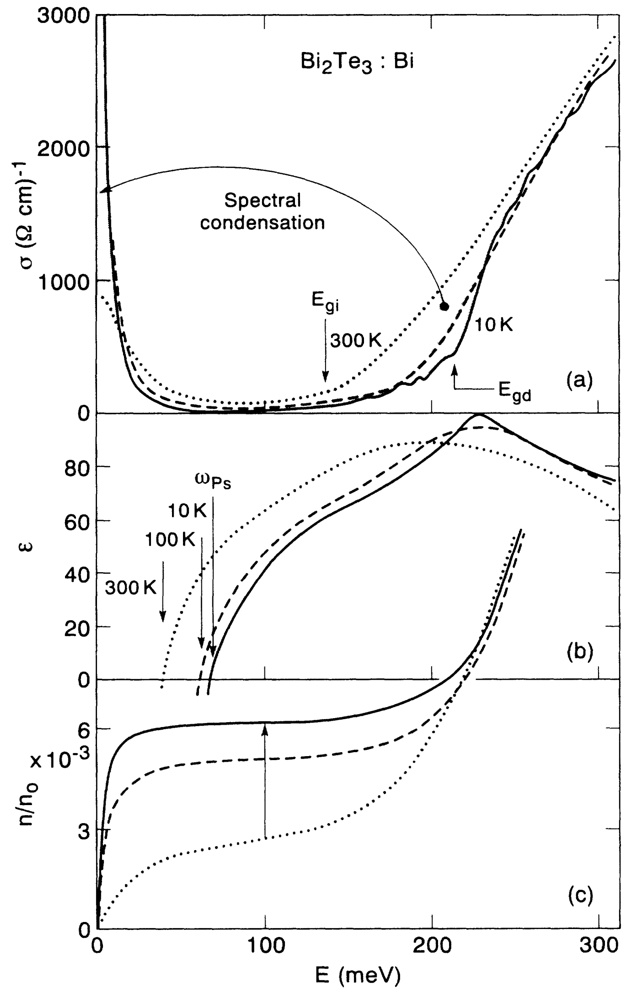

FIG. 2. (a) Real part of the conductivity σ for the same sample as in Fig. 1(a) as a function of E at three temperatures T (dotted curve, 300 K; dashed curve, 100 K; solid curve, 10 K). The arrow labeled E_{gi} denotes a weak absorption edge at $T=10$ K (probably the indirect energy gap), while the second arrow identifies a strong feature E_{gd} (probably the direct gap). The shaded areas indicate the region near the gaps which loses spectral weight and the zero-frequency mode into which the spectral condensation occurs on cooling. (b) Real part of the dielectric constant ϵ with arrows indicating the zero crossings for three values of T which confirm our values of ω_{Ps}, and the values of $\epsilon_H \sim 90$ near the gap region. (c) Normalized carrier densities n/n_0 calculated from the integrals over σ (same notation for the curves above). At $E=100$ meV, with decreasing T, the large density increase in metallic states can be seen, as indicated by the arrow, while at higher E the curves come back together, indicating that the density shifts with cooling from above E_g to below.

Shubnikov–de Haas oscillation amplitude.[9] Assuming one hole for each excess Bi atom, the dopant concentration per formula unit is 0.003 (i.e., $Bi_{2.003}Te_{2.997}$).

We now consider the nonconducting states near the energy gap by analyzing the conductivity σ at higher E. We have carried out measurements over a range from a few meV to about 3 eV and have performed a Kramers-Kronig transformation[2,3] of the R data. We use a conventional extrapolation at high frequency and a Drude interpolation to the measured dc resistivity [see inset in Fig. 1(b)] at low frequency. We thus obtain the real part of the conductivity σ and the real part of the dielectric constant ϵ shown in Fig. 2. Our R at higher frequencies than those shown in Fig. 1(a) is similar to that measured previously.[7,11] In agreement with previous measurements,[7,12,13] we find strong phonon absorption at low frequencies, which, for clarity, we have subtracted (using the Drude form) from the quantities shown in Fig. 2. (We find that the phonons have a relatively small spectral weight.)

The conductivity spectra in Fig. 2(a) show the change in spectral weight near the energy gap as a shaded area, with an arrow indicating the shaded region near zero frequency where this weight reappears on cooling. We find a clear separation between the metallic states and the states above the band edge. We can measure the spectral weight changes quantitatively in these different parts of the spectrum with an integral of σ over frequency ν,

$$\omega_{Ps}^2 = 8\int_0^E \sigma d\nu \ . \quad (3)$$

If the cutoff E is taken to ∞, we have the sum rule which describes the total electronic density. The partial sum[2–4] is shown in Fig. 2(c), where n, calculated using Eqs. (1) and (2), is normalized to the density of atoms in a formula unit n_0 and plotted as a function of the upper cutoff E of the integral. Figure 2(c) confirms that the weight in the zero-frequency mode (included at $E \sim 100$ meV) increases strongly with decreasing T, as indicated by the arrow. In addition, however, it shows that the curves come back together by $E \sim 250$ meV, indicating that the decrease in weight above the energy gap balances the increase in the metallic mode. The values for n at $E = 100$ meV in Fig. 2(c) are in agreement with the values in Fig. 1(b), and also agree with the values from the zero crossings in the real part of the dielectric constant ϵ shown in Fig. 2(b). The values of $\epsilon \sim 90$ just below the band edge agree with the ϵ_H used to fit the raw R, indicating again that the data analysis is self-consistent.

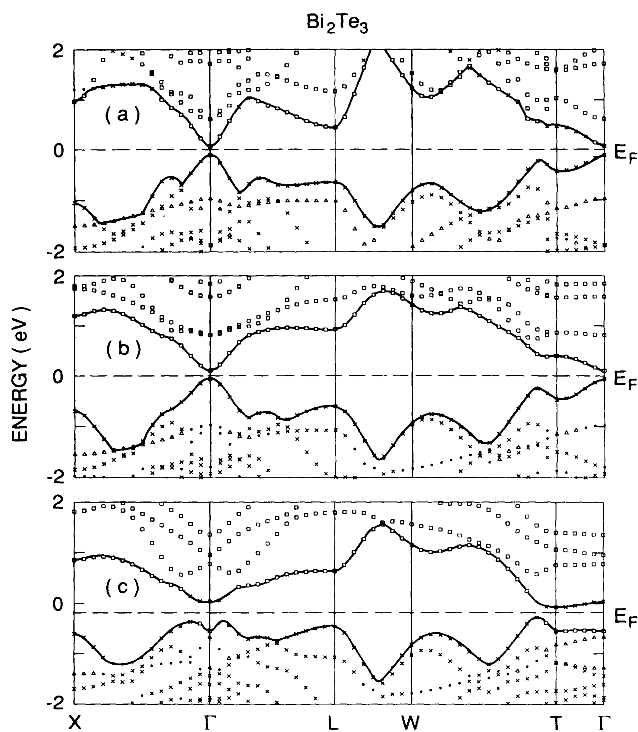

FIG. 3. Comparison of (a) scalar-relativistic LAPW, (b) scalar-relativistic tight-binding (TB), and (c) fully relativistic TB [with the spin-orbit parameters $\xi_{6p}(\mathrm{Bi}) = 1.12$ eV, $\xi_{5p}(\mathrm{Te}) = 0.57$ eV] bands near E_F for rhombohedral Bi_2Te_3, using the zone-labeling notation of Togei and Miller (Ref. 18). The triangles, squares, and crosses identify LAPW (TB) states with at least 20% (50%) Te(1), Bi_2, and $[Te(2)]_2$ orbital weight, respectively, on the inequivalent sites of the five-layer Te(2)-Bi-Te(1)-Bi-Te(2) sandwiches.

Several aspects of the materials need to be understood in order to formulate a model of the physics involved in the T-dependent properties. These include the degree of compensation,[5,6] the strong electron-phonon interactions,[6] and the thermal excitations within the intrinsic band structure.[6–13] Since the band structure is a fundamental component, we focus on it here.

Our calculations of the band structure, summarized in Fig. 3, show that a small band gap is expected for Bi_2Te_3. An accurate calculation is required because this gap is small. As shown in Fig. 3(a), the results of a scalar-relativistic linear-augmented-plane-wave (LAPW) band calculation[17] for this compound predict that it is a direct-gap ($E_{gd} \sim 0.17$ eV) semiconductor in the absence of spin-orbit-coupling effects. In particular, these results show that the filled valence and empty conduction bands have predominant Te($5p$) and Bi($6p$) orbital character, respectively. Consequently, this calculation provides a simple chemical understanding of the band ordering and gap origin in Bi_2Te_3 that is absent in previous calculations, where spin-orbit coupling was essential for the gap-formation process.[18] According to the present scalar-relativistic LAPW results, the states at both the valence-band maximum ($\Gamma_{1'}$) and the conduction-band minimum (Γ_1) are spatially nondegenerate, so that the relevant spin-orbit effects will involve band shifts rather than splittings.

We find that the transitions near the band edge are strongly affected by spin-orbit coupling and arise from indirect transitions, with a direct gap at slightly higher energy. To show this, we have carried out an accurate tight-binding (TB) fit (rms error ~ 0.24 eV) to the LAPW results for the entire 20-band s-p valence–conduction-band manifold (~ -14 eV to $+5$ eV). The accuracy of the results near E_F is illustrated in Fig. 3(b). Spin-orbital effects have been added to this TB model using the atomic spin-orbit parameters of Herman and Skillman.[19] As

shown in Fig. 3(c), this introduces a dramatic change in the band ordering and connectivity near E_F. In particular, the large Bi(6p) spin-orbit parameter (~ 1.1 eV) reverses the scalar-relativistic ordering of the Γ_1 and $\Gamma_{1'}$ states. The resultant band uncrossings at neighboring **k** points change Bi_2Te_3 from a direct-gap to an indirect-gap semiconductor. According to these model TB results, reduced direct (~ 0.08 eV) and indirect (~ 0.05 eV) gaps occur at adjacent (uncrossed) valence- and conduction-band edges in the reflection planes of the D_{3d}^5 space group near the ΓT line. While these band features are believed to be qualitatively correct, it will require a fully relativistic first-principles calculation of the Bi_2Te_3 band structure in order to obtain a quantitative understanding of these important and novel features near E_F. We suggest that two features in the spectra of Fig. 2(a) at $T=10$ K are a gap at $E_{gi}=(150\pm 20)$ meV (probably indirect, since the absorption near it is weak) and a sharp absorption increase at $E_{gd}=(220\pm 20)$ meV (probably a direct gap). These structures become less well defined as the spectral weight in this energy range increases with T, but are in agreement with previous measurements.[7] Our measurements are not sufficiently detailed to confirm the possibility of heavy-mass Fermi-surface pockets above the chemical potential which have been assumed previously,[6] though the band results are consistent with this possibility.

In conclusion, we have emphasized the observation that cooling this layered metal causes a spectral condensation of significant magnitude—a result that is contrary to the expectation for a simple metal that the plasma frequency would be essentially constant and opposite to that for a lightly doped semiconductor, which would show carrier freeze-out. We show that this condensation arises because of a shift from above-gap states to metallic states.

We wish to acknowledge helpful discussions with A. J. Millis, P. B. Littlewood, and K. B. Rabe, and we thank R. A. Laudise for crystal growth.

[1]See, for example, J. A. Wilson, F. J. DiSalvo, and S. Mahajan, Adv. Phys. **24**, 117 (1975).

[2]See, for example, *Physical Properties of High Temperature Superconductors,* edited by D. M. Ginsburg (World Scientific, Singapore, 1989), particularly the review by T. Timusk and D. B. Tanner, p. 339.

[3]F. Stern, in *Solid State Physics,* edited by F. Seitz and D. Turnbull (Academic, New York, 1963), Vol. 15, p. 1.

[4]G. A. Thomas, J. Orenstein, D. H. Rapkine, M. Capizzi, A. J. Millis, R. N. Bhatt, L. F. Schneemeyer, and J. V. Waszczak, Phys. Rev. Lett. **61**, 1313 (1988); J. Orenstein, G. A. Thomas, A. J. Millis, S. L. Cooper, D. H. Rapkine, T. Timusk, L. F. Schneemeyer, and J. V. Waszczak, Phys. Rev. B **42**, 6342 (1990); K. Kamaras, S. L. Herr, C. D. Porter, N. Tache, D. B. Tanner, S. Etemad, T. Venkatesan, and E. Chase, Phys. Rev. Lett. **64**, 84 (1990).

[5]N. F. Mott and E. A. Davis, *Electronic Processes in Non-Crystalline Materials* (Oxford University, London, 1979).

[6]*Physics of Semimetals and Narrow Gap Semiconductors,* edited by D. L. Carter and R. T. Bates (Pergamon, Oxford, 1971); *Electrons and Phonons in Layered Crystal Structures,* edited by T. J. Wieting and M. Schluter (Reidel, Boston, 1977); for *p*-type Bi_2Te_3, J. R. Drabble, Prog. Semicond. **7**, 45 (1963); J. R. Drabble, Proc. Phys. Soc. London **72**, 380 (1958); H. J. Goldsmit, *ibid.* **71**, 633 (1958); R. Mansfield and W. Williams, *ibid.* **72**, 733 (1958); B. A. Efimova, I. Ya. Korenblum, V. I. Novikov, and A. G. Ostroumov, Fiz. Tverd. Tela (Leningrad) **9**, 2544 (1967) [Sov. Phys. Solid State **9**, 2004 (1967)]; N. Chand, T. Henderson, J. Klem, W. T. Masselink, R. Fisher, Y. C. Chang, and H. Moroc, Phys. Rev. B **30**, 4481 (1984).

[7]B. L. Evans, *Optical Properties of Layer Compounds* (Reidel, Dordrecht, 1976); *n*-type $In_xGa_{1-x}Sb$, M. Cardona, J. Phys. Chem. Solids **17**, 336 (1961).

[8]C. H. Champness and A. L. Kipling, Can. J. Phys. **44**, 769 (1966).

[9]H. Kohler, Phys. Status Solidi B **74**, 591 (1976); **75**, 441 (1976). For a discussion of anisotropy and the Hall effect, see, for example, R. Wolfe, in *Thermoelectricity,* edited by P. H. Egli (Naval Research Laboratory, Washington, D.C., 1958), p. 106. Our measurements are with current and voltage in the planes and magnetic field perpendicular.

[10]R. B. Mallinson, J. A. Rayne, and U. W. Ure, Jr., Phys. Rev. **175**, 1049 (1968); C. B. Satterthwaite and R. W. Ure, Jr., *ibid.* **108**, 1164 (1957).

[11]D. L. Greenaway and G. Harbeke, J. Phys. Chem. Solids **26**, 1585 (1965).

[12]V. Wagner, G. Dolling, B. M. Powell, and G. Landwehr, Phys. Status Solidi B **85**, 311 (1978).

[13]W. Richter, H. Kohler, and C. R. Becker, Phys. Status Solidi B **84**, 619 (1977); K. H. Unkelbach, C. Becker, H. Kohler, and A. von Middendorff, *ibid.* **60**, K41 (1973).

[14]R. A. Laudise, W. A. Sunder, R. L. Barnes, R. J. Cava, and T. Y. Kometani, J. Cryst. Growth **94**, 53 (1989).

[15]R. W. G. Wyckoff, *Crystal Structures* (Krieger, Malabar, FL, 1986); Vol. 2; S. Nakajima, J. Phys. Chem. Solids **24**, 479 (1963).

[16]P. B. Allen, Phys. Rev. B **3**, 305 (1971); J. H. Kim, K. Levin, R. Wentzcovitch, and A. Auerbach, *ibid.* **40**, 11 378 (1989).

[17]L. F. Mattheiss and D. R. Hamann, Phys. Rev. B **33**, 823 (1986).

[18]P. M. Lee and L. Pincherele, Proc. Phys. Soc. London **81**, 461 (1963); F. Borghese and E. Donato, Nuovo Cimento **53**, 283 (1968); S. Katsuki, J. Phys. Soc. Jpn. **26**, 58 (1969); R. Togei and G. R. Miller, in *Physics of Semimetals and Narrow Gap Semiconductors* (Ref. 6), p. 349; E. V. Oleshko and V. N. Korolyshin, Fiz. Tverd. Tela (Leningrad) **27**, 2856 (1985) [Sov. Phys. Solid State **27**, 1723 (1985)].

[19]F. Herman and S. Skillman, *Atomic Structure Calculations* (Prentice-Hall, Englewood Cliffs, NJ, 1963).

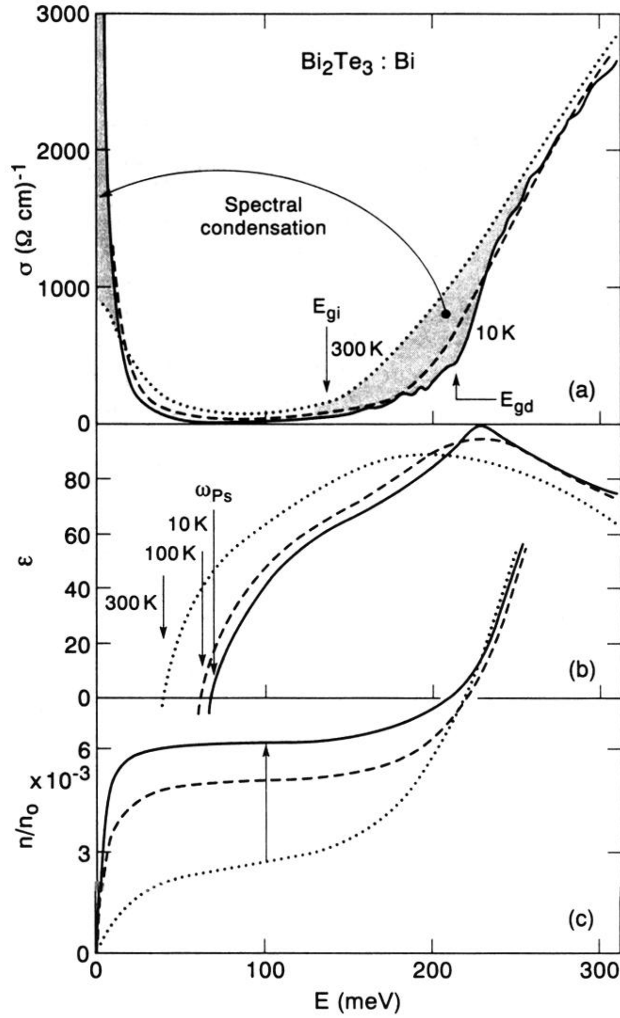

FIG. 2. (a) Real part of the conductivity σ for the same sample as in Fig. 1(a) as a function of E at three temperatures T (dotted curve, 300 K; dashed curve, 100 K; solid curve, 10 K). The arrow labeled E_{gi} denotes a weak absorption edge at $T=10$ K (probably the indirect energy gap), while the second arrow identifies a strong feature E_{gd} (probably the direct gap). The shaded areas indicate the region near the gaps which loses spectral weight and the zero-frequency mode into which the spectral condensation occurs on cooling. (b) Real part of the dielectric constant ϵ with arrows indicating the zero crossings for three values of T which confirm our values of ω_{Ps}, and the values of $\epsilon_H \sim 90$ near the gap region. (c) Normalized carrier densities n/n_0 calculated from the integrals over σ (same notation for the curves above). At $E=100$ meV, with decreasing T, the large density increase in metallic states can be seen, as indicated by the arrow, while at higher E the curves come back together, indicating that the density shifts with cooling from above E_g to below.